Patch-based Histopathological Images for Non-Hodgkin Lymphoma Detection using Voting CNN with Layer Freezing

Ardytha Luthfiarta, Ika Novita Dewi*, *Member, IAENG*, Erwin Yudi Hidayat, Catur Supriyanto, Permana Langgeng Wicaksono Ellwid Putra, and Ahmed Sabeeh Yousif

Abstract— **Non-Hodgkin Lymphoma (NHL) is characterized by its diverse subtypes of lymphoid malignancies, presenting challenges for accurate diagnosis due to the variability in tissue morphology and immunophenotypic profiles. This research proposes a novel automated approach for NHL subtype classification using histopathological images, integrating a combination of patch-based analysis with a voting ensemble of Convolutional Neural Networks (CNN). Pre-trained CNN models such as DenseNet169, MobileNetV2, and NASNetMobile were enhanced using a layer-freezing technique to preserve learned low-level features while fine-tuning higher-level layers for improved specificity in NHL detection. A majority voting mechanism aggregates predictions from individual image patches, enhancing classification robustness. The proposed model was evaluated on the IICBU 2008 Lymphoma image dataset, achieving a classification accuracy of 99.11% and an F1-score of 99.11%, surpassing previous methods. This approach demonstrates significant potential in improving the accuracy, efficiency, and clinical applicability of automated NHL subtype classification from histopathological images.**

Index Terms—Convolutional Neural Network, Histopathological Images, Image patching, Non-Hodgkin Lymphoma

I. INTRODUCTION

LYMPHOMA is a cancer that develops in the lymphatic system, a vital part of the body's immune defense. Lymphoma has two main classifications: Hodgkin lymphoma (HL) and non-Hodgkin lymphoma (NHL) [1]. HL typically begins in a single lymph node or group of adjacent nodes and then spreads to nearby lymph nodes. In contrast, NHL encompasses diverse lymphoid malignancies with unique morphological and immunophenotypic characteristics. The incidence of NHL has been increasing globally, underscoring the need for early and accurate diagnosis to ensure effective treatment and better patient outcomes.

A comprehensive analysis of NHL epidemiology reveals that approximately 200,000 deaths occur globally each year, with age-standardized mortality rates exhibiting relative consistency across various regions [2]. Despite advancements in medical imaging and diagnostic technologies, distinguishing between NHL subtypes remains challenging due to the disease's complexity and variability.

The histopathological analysis of tissue samples remains the gold standard for diagnosing NHL [3]. However, this process is challenging due to the laborious process and requires highly skilled pathologists to accurately interpret the intricate details of tissue structure and cellular morphology. Histopathological images of NHL present significant challenges due to their high variability in tissue morphology and staining patterns across different NHL cases. This variability can obscure the subtle features needed to distinguish between different NHL subtypes when analyzing the whole-slide image [4]. Early and precise diagnosis of NHL is critical for guiding treatment strategies and enhancing the quality of patient care, as timely identification of specific subtypes can lead to more targeted therapies and better prognosis. Delays or inaccuracies in diagnosis may result in suboptimal treatment strategies, potentially reducing survival rates and increasing the burden on healthcare systems [5]. Thus, there is an urgent need for automated assistance for pathologists in enhancing diagnostic accuracy and efficiency.

The quality and clarity of histopathological images are crucial for accurate interpretation, aiding in medical research, education, and the development of diagnostic tools. However, the large size of histopathological images can pose computational challenges regarding storage, processing, and analysis [3]. A patch-based approach overcomes this problem by dividing large histopathological images into smaller, manageable patches, allowing for a more detailed and localized analysis [4]. This method allows for identifying localized features that may indicate NHL, thereby improving the accuracy of the diagnostic process [5]. Additionally, this approach reduces the computational load and memory requirements, making the training process more efficient and feasible on standard hardware [6]. A patch-based approach for analyzing histopathological images has been successfully implemented to handle large image sizes and extract meaningful information efficiently, such as breast cancer classification [7], uterine cervical and endometrial cancer subtypes classification [8], cellular morphology analysis [9], and invasive ductal carcinoma classification [10].

Manuscript received July 5, 2024; revised January 21, 2025. This research was supported by Office of Research and Community Service Universitas Dian Nuswantoro, which provided research funding in 2023 (109/A.38-04/UDN-09/XI/2023).

Ardytha Luthfiarta is a lecturer of Department of Informatics Engineering, Universitas Dian Nuswantoro, Indonesia. (e-mail: ardytha.luthfiarta@dsn.dinus.ac.id)

Ika Novita Dewi is a lecturer of Department of Information System, Universitas Dian Nuswantoro, Indonesia. (ikadewi@dsn.dinus.ac.id)

Erwin Yudi Hidayat is a lecturer of Department of Informatics Engineering, Universitas Dian Nuswantoro, Indonesia. (erwin@dsn.dinus.ac.id)

Catur Supriyanto is a lecturer of Department of Informatics Engineering, Universitas Dian Nuswantoro, Indonesia. (catur.supriyanto@dsn.dinus.ac.id)

Permana Langgeng Wicaksono Ellwid Putra is an undergraduate student of Department of Informatics Engineering, Universitas Dian Nuswantoro, Indonesia. (langgeng86@gmail.com)

Ahmed Sabeeh Yousif is a lecturer of Technical College of Management Mousl, Northern Technical University, Iraq. (Ahmedsabeeh123@ntu.edu.iq)

Recent developments in deep learning, particularly CNN, have demonstrated significant potential in medical imaging [11]. Deep learning algorithms, including convolutional neural networks, are used to process grid-structured data like images [12]. The networks use convolutional layers to automatically learn and detect important features directly from raw input data, without requiring manual feature engineering. Each convolutional layer extracts increasingly complex features, from simple attributes like edges and textures to more complex patterns shapes and objects. This hierarchical feature learning makes CNN particularly well-suited for tasks specifically image classification [13], image detection [14], image segmentation [15], and anomaly detection [16]. Pretrained CNN, which are models initially trained on extensive datasets such as ImageNet, have exhibited impressive success in various image classification tasks Given their capacity for learning generalizable hierarchical features [17]. In the context of NHL detection, pre-trained models such as MobileNetV2, DenseNet169, and NASNetMobile can be used to extract features from the histopathological images. Having been trained on millions of natural images, these models can recognize complex patterns and subtle details in medical images, which are essential for accurate diagnosis [18]. Fine-tuning these pre-trained models on NHL-specific data enables the adaptation of learned features for the particular task of NHL subtype classification. By leveraging the strengths of CNN in hierarchical feature learning, the models can be optimized to detect the morphological variations present in histopathological images of NHL, thereby improving diagnostic accuracy and efficiency [19].

Layer freezing is an effective technique for enhancing the performance of pre-trained CNN models [20]. It leverages the strengths of pre-trained networks to optimize the training process, making it particularly valuable for medical image analysis where annotated datasets are frequently limited [21]. In this approach, the early layers of the network, that capture fundamental image features like edges and textures, remain unchanged during training, while the following layers are fine-tuned for the specific task [22]. The model retains generic, low-level features by freezing the initial layers and concentrates on learning higher-level, domain-specific features from the histopathological patches [23]. To further improve classification accuracy, a majority voting mechanism can be employed [24]. This voting mechanism operates by classifying each patch independently and then determining the final classification of the whole image based on the majority vote of these individual patch predictions [25]. Aggregating multiple predictions in this manner ensures that the final decision is informed by a broader context, thereby reducing the impact of any single misclassified patch. As a result, the model gains robustness to noise and artifacts present in individual patches, leading to more reliable and accurate classification outcomes.

This research aims to develop a robust and efficient CNN-based model for classifying NHL subtypes using the IICBU 2008 Lymphoma Image Dataset [26]. Existing CNN-based approaches for NHL classification often face significant challenges, such as overfitting due to the limited availability of annotated datasets and difficulties in handling noise and artifacts in histopathological images. Additionally, the large size of whole-slide images requires substantial memory and processing power, limiting the feasibility of these methods in clinical settings. These limitations can reduce both the accuracy and robustness of classification outcomes.

To address these challenges, we present a new approach integrating a patch-based analysis with a majority voting mechanism and layer freezing technique. This approach improves classification accuracy and robustness and enhances computational efficiency by focusing on smaller, manageable patches rather than whole-slide images. Layer freezing helps prevent overfitting by retaining the essential low-level features learned from pre-trained models. Meanwhile, the majority voting strategy aggregates patch-level predictions to provide a more reliable final classification, thereby mitigating the impact of any single misclassified patch. This research makes three significant contributions. First, we introduce a comprehensive approach for detecting NHL in histopathological images using a patch-based method and pre-trained CNN models, overcoming the limitations of whole-slide analysis by focusing on localized features. Second, we demonstrate the effectiveness of layer freezing in improving pre-trained models' performance for NHL classification, addressing challenges like overfitting and optimizing feature learning for this specific medical application. Third, we introduce a majority voting strategy to aggregate patch-level predictions, which mitigates the impact of noise and misclassifications by considering a broader context for the final diagnosis, thus improving the overall robustness and accuracy.

II. RELATED WORK

The IICBU 2008 Lymphoma Image Dataset has been instrumental in advancing research on the automated detection and classification of lymphoma in histopathological images. This dataset comprises diverse images representing different lymphoma subtypes, providing a valuable resource for developing and evaluating machine learning models. Several studies have leveraged the IICBU 2008 Lymphoma Image Dataset for histopathological image analysis and classification research. Bai et al. (2019) focus on leveraging hierarchical local information and the GoogLeNet model to improve the classification accuracy of NHL in pathological images [27]. By integrating patch-based approaches and sophisticated feature extraction techniques from GoogLeNet, the study aims to capture localized patterns indicative of different NHL subtypes, thereby enhancing the diagnostic process through better feature representation and classification performance. The proposed model demonstrates achieved an improved overall accuracy of 99.1% and an area under the receiver operating characteristic curve of 99.8%. Classifying lymphoma images utilizing both morphological and non-morphological descriptors proposed by Nascimento et al. (2018). The study involves extracting morphological features extracted from detected nuclei and non-morphological features derived from statistical metrics of RGB color model and grayscale images. The experiments conducted by support vector machines (SVM) resulted in 98.13% accuracy, 98.33% precision, 98.00% recall, and 98.16% F1 score [28]. Martins et al. (2019) explore classifying lymphoma images using color feature extraction

combined with a polynomial algorithm. The proposed method demonstrates significant improvements in the classification of lymphoma images. Integrating fractal features and the polynomial classifier achieves high accuracy in distinguishing between lymphoma lesions, providing valuable support in clinical diagnostics. The conducted experiments resulted in performance of accuracy rates between 91% and 97% [29]. Malignant lymphoma cell detection applied by Hamdi et al. (2023) by using an XGBoost network that combines MobileNet-VGG16 and handcrafted features such as color, shape, and texture features achieved an accuracy of 99.8% [30].

Deep learning, particularly CNN, has significantly advanced the field of medical image analysis. CNN automatically learn hierarchical features from raw image data, eliminating the need for manual feature extraction. Transfer learning [31], which involves fine-tuning pre-trained models on specific tasks, has further enhanced the performance of CNN in medical image analysis. Pre-trained models, such as VGG, ResNet, Inception, and DenseNet, have demonstrated their ability to effectively transfer learning from large-scale image datasets like ImageNet to specific medical imaging tasks, including histopathological image analysis [32]. DenseNet, known for its dense connectivity patterns, has performed remarkably well in medical image classification. For instance, Zhang et al. (2019) used a pre-trained DenseNet-121 model for breast cancer histopathological image classification, achieving high accuracy and robustness. The model's ability to reuse features across layers allows for better representation learning, crucial for detecting subtle patterns in histopathological images [1].

Patch-based methods involve dividing large histopathological images into smaller patches, which are then analyzed independently. This approach mitigates the computational challenges posed by high-resolution images. Each patch is classified separately, and techniques like majority voting are used to aggregate patch-level predictions into a final classification for the whole image. This method has proven effective in capturing localized features critical for accurate diagnosis. Several studies have demonstrated the effectiveness of patch-based approaches in various histopathological tasks, including tissue classification, object detection, segmentation, and outcome prediction. Hirra et al. (2021) propose a patch-based deep learning framework for breast cancer classification, effectively capturing spatial information and local features within histopathological images. The model can learn discriminative patterns indicative of different cancer subtypes by dividing the images into smaller patches and employing deep CNN. The proposed model demonstrated 86% accuracy on a whole slide histopathology image dataset containing images from four distinct data cohorts [7]. Ciga et al. (2021) addressed the need for more robust and efficient methods to analyze large-scale histopathological images for accurate cancer diagnosis in whole slide images (WSIs) by recognizing challenges such as limited contextual information, computational inefficiency, and model scalability issues. This research proposed a negative data sampling strategy, drastically reducing the false positive rate (25% of false positives versus 62.5%), indicating that classification performances of image patches versus WSIs are inversely related when using the same negative data sampling strategy [34]. Moscalu et al. (2023) explore the latest advancements, challenges, and potential applications of histopathological image analysis and predictive modeling in digital pathology. This study concluded that pathologists can extract valuable insights from digital pathology data by leveraging computational techniques and machine learning algorithms, facilitating early detection, precise risk stratification, and targeted therapy selection [35].

Layer freezing is a technique where the weights of the initial layers of the pre-trained network are held constant during fine-tuning. This performance enables the model to preserve the generic, low-level features from the large-scale dataset while learning higher-level, domain-specific features from the histopathological patches. This strategy has improved training efficiency and generalization performance in medical image classification tasks. Layer freezing and majority voting in pre-trained CNN models is a relatively new approach. Ahmed et al. (2023) optimized the transfer learning process by investigating various layer-freezing techniques of the pre-trained model, such as Inception-V3 and VGG-16. Layer freezing in the context of transfer learning involves selecting specific layers of a pre-trained neural network and preventing them from being updated during the training process on a new dataset [35]. The early layers of the network (closer to the input layer) are frozen to capture basic and general features like edges, textures, and patterns. The later layers (closer to the output layer), which capture more complex and specific features, are left unfrozen and are fine-tuned to allow the model to adapt these layers to the specific patterns and characteristics of histopathological images. The findings demonstrate that an optimal freezing strategy significantly improves the classification performance compared to training a model from scratch or using all layers unfrozen. Panigrahi et al. (2023) applied VGG16, VGG19, ResNet50, InceptionV3, and MobileNet, then implemented a strategic layer freezing approach to enhance the performance and efficiency of the classification model. The proposed approach not only improves classification performance but also enhances training efficiency. Experimental results showed that ResNet50 achieved substantially higher performance compared to the selected fine-tuned DCNN models and the proposed baseline model, with an accuracy of 96.6%, a precision of 97%, and a recall of 96%. [36]. Wang et al. (2023) investigates the application of various depths of the ResNet architecture to determine the impact of network depth on the performance of histopathologic cancer detection and found that freezing most layers does not enhance the accuracy or efficiency of transfer learning, and the performance of both transfer strategies is largely determined by the data type [37].

Integrating layer freezing and majority voting with pre-trained CNN models is promising, aiming to improve the accuracy and robustness of NHL detection in histopathological images. These approaches leverage pre-trained CNN to enhance classification performance and robustness. Saha et al. (2023) explore the efficacy of various pre-trained CNN models such as VGG-16, VGG-19, Restnet50, Inception-V3, Densnet, Xception, MobileNetV2, Alexnet, Lenet, and majority voting was employed in classification for identifying and predicting monkeypox from medical images. The results indicate varying performance

across different models and classification tasks. Majority voting achieved the highest accuracy (97%) in the monkeypox vs. chickenpox classification. MobileNetV2 also performed well (96%) in distinguishing monkeypox from normal cases. Xception and LeNet achieved lower accuracies of 79% (monkeypox vs. measles) and 80% (monkeypox vs. all), respectively [38]. Pal et al. (2024) investigate the application of ensemble learning techniques for detecting brain tumors from medical images to enhance the accuracy and robustness of brain tumor detection by combining multiple machine-learning models. Several pre-trained CNN models, such as VGG16, ResNet50, and InceptionV3, are used as base classifiers within the ensemble. The ensemble framework utilizes a majority voting mechanism to combine the predictions from the individual CNN models. Each image's final classification decision is based on the most common prediction among the base classifiers. The proposed model achieved a high detection accuracy of 98% with a low false positive rate after being trained and evaluated on a standard brain tumor dataset of 3000 brain MRI images [39].

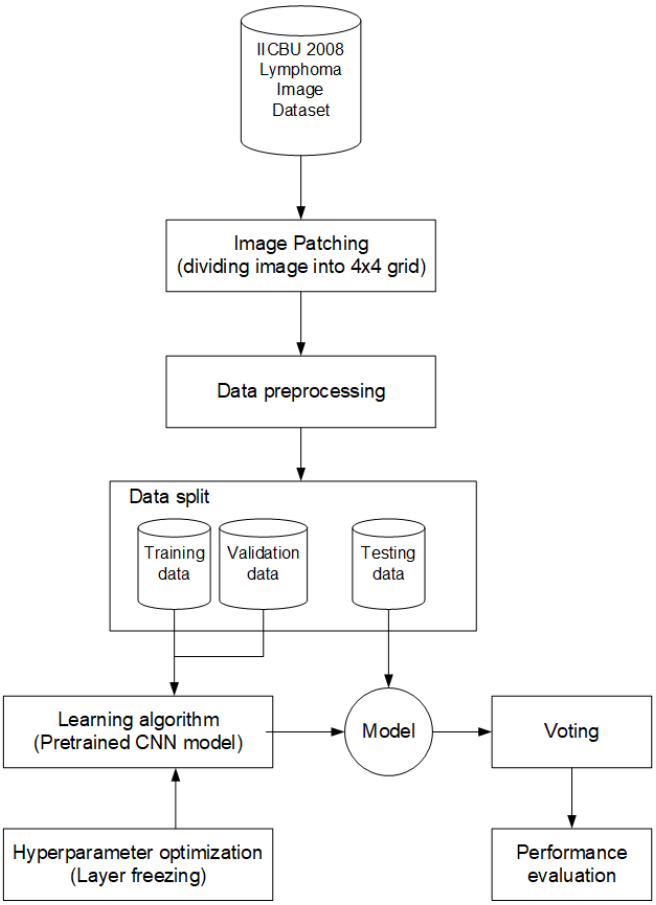

Fig. 1. Research flow

III. PATCH-BASED VOTING CNN WITH LAYER FREEZING

This research consisted of several steps, as shown in Fig. 1. The research starts with dataset preparation, specifically utilizing the IICBU 2008 Lymphoma Image Dataset. Each histopathological image is divided into a 4x4 grid, creating 16 patches per image to allow the model to focus on localized tissue features. These patches are then subjected to data preprocessing, where the patches are grouped and formatted into arrays suitable for further processing. Following preprocessing, a pre-trained CNN model, such as DenseNet169, is employed with layer freezing to retain general feature extraction capabilities while fine-tuning only the final layers. During testing, a majority voting algorithm aggregates predictions from the patches, selecting the most common class label as the final decision. The model's performance is then evaluated using metrics like accuracy and F1-score to assess its effectiveness in classifying NHL subtypes.

A. Dataset

This research utilized the IICBU 2008 lymphoma image dataset, which has been previously published. The dataset consists of 374 histopathological images of NHL in 32-bit TIFF format with 1,388 x 1,040 pixels. Examples of images from this dataset can be seen in Fig. 2. The NHL dataset includes images from three distinct lymphoma classes: chronic lymphocytic lymphoma (113 images), follicular lymphoma (139 images), and mantle cell lymphoma (122 images). All three types of lymphomas are aggressive B-cell lymphomas with high malignancy rates.

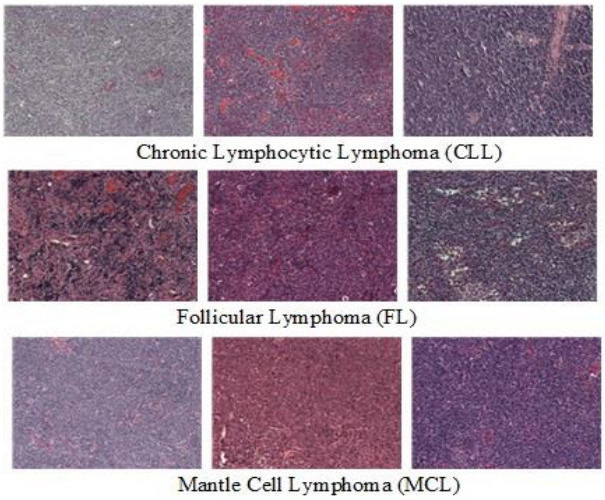

Fig. 2. Example of Lymphoma Sub-Type Images: CLL, FL, MCL

B. Proposed architecture

The proposed architecture of patch-based histopathological images using voting CNN with layer freezing for NHL detection shown in Fig. 3. The experiments were conducted in three main steps: patch-based histopathological images, implementation of CNN Pre-trained models, and layer freezing with majority voting.

Patch-based Histopathological Images

The method begins by dividing each whole-slide histopathological image into 16 equally-sized patches. This process, known as image patching, facilitates the analysis of large images by breaking them down into smaller, more manageable segments. Each patch retains the critical local information needed for classification, ensuring that even subtle histopathological features are captured given the partition of the image I with $H \times W$ dimensions. Each patch P_i will have dimensions of $\frac{H}{4} \times \frac{W}{4}$. This approach ensures that the model can capture localized histopathological features more effectively, improving the granularity and accuracy of the analysis.

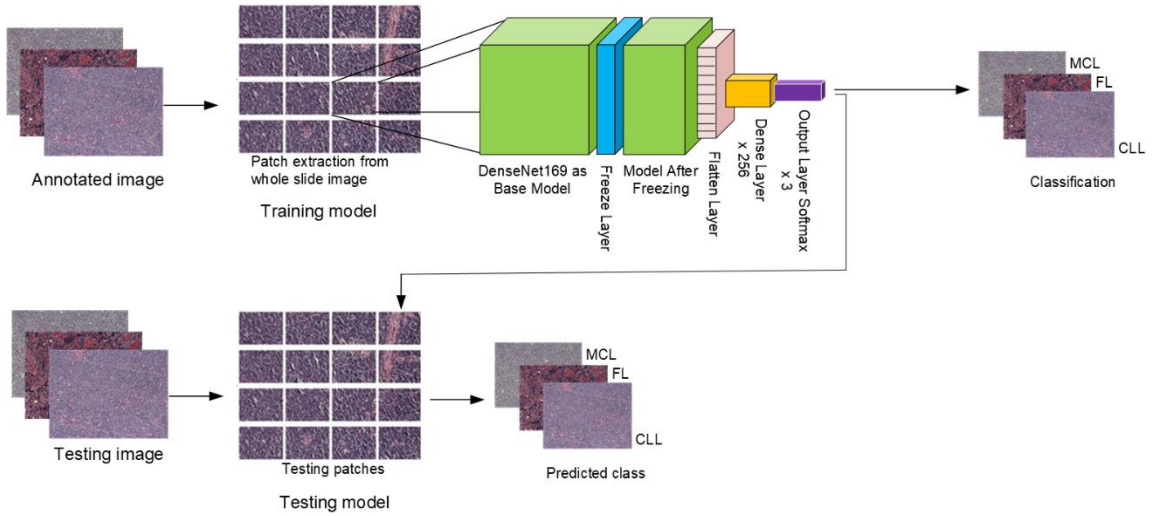

Fig. 3. Proposed architecture

Implementation of CNN Pre-trained models

This research employs pre-trained CNN models, specifically MobileNetV2, DenseNet169, and NASNetMobile, to extract features from the patches. MobileNetV2 is known for its mobile efficiency and embedded vision applications, utilizing depth-wise separable convolutions to reduce the number of parameters. DenseNet169, with its dense connectivity pattern, ensures efficient gradient flow and feature reuse, making it suitable for complex image recognition tasks. NASNetMobile, designed through Neural Architecture Search, provides an optimized architecture that balances accuracy and computational efficiency. These models, pre-trained on large image datasets, are fine-tuned on the histopathological patches to adapt to the specific task of NHL subtype classification. The configuration setting of the pre-trained models is explained in Table I.

TABLE I
PARAMETER SETTING

Configuration	Setting
Input Size	255x255 pixels
Activation Function	ReLu
Optimizer	Adam, SGD, RMSprop, AdamW, Adadelta, Adegrad, Adamax, Nadam, and Ftrl
Batch Size	8, 16, and 32
Learning rate	0,001 and 0,0001

Layers Freezing and Majority Voting

Layer freezing was conducted using two scenarios: layer freezing on the back layers and layer freezing on the front layers. Layer freezing on the back layers means the weights of these layers remain unchanged during training while the earlier layers (closer to the input) are updated. Freezing the back layers helps preserve the learned features from the pre-trained model and focuses the training process on fine-tuning the initial layers. This layer freezing can be particularly effective when the initial layers already capture the general features well, and the model needs to adapt to specific features in the new dataset. Layer Freezing on the front layers approach keeps the weights of the initial layers intact while allowing the later layers to be updated during training. Freezing the front layers can be advantageous when the initial layers contain fundamental features like edges and textures that are useful across various datasets. At the same time, the deeper layers need to learn the specific characteristics of the target dataset.

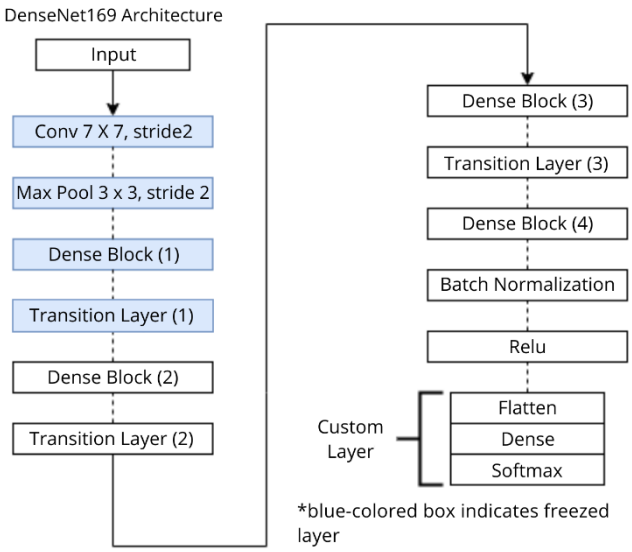

Fig. 4. DenseNet169 Architecture with Layer Freezing

TABLE II
ACCURACY OF PRE-TRAINED CNN MODEL

Optimizer	MobileNetV2	DenseNet169	NASNetMobile
Adam	0,863	0,8675	0,8641
SGD	0,8619	0,902	0,8753
RMSprop	0,8541	0,8953	0,8719
AdamW	0,8664	0,8675	0,8653
Adadelta	0,843	0,882	0,8686
Adegrad	0,8742	0,9042	0,8708
Adamax	0,8486	0,8898	0,8575
Nadam	0,8441	0,8719	0,8675
Ftrl	0,843	0,863	0,8597

The illustration of DenseNet169 architecture incorporating a layer-freezing strategy presented in Fig. 4. The initial part of the architecture begins with a convolutional layer applying a 7×7 filter with a stride of 2, followed by a max pooling layer with a 3×3 filter to reduce spatial dimensions and extract low-level features. Subsequent dense blocks are interspersed with transition layers, where each dense block consists of multiple convolutional layers that concatenate outputs from all preceding layers, promoting feature reuse and efficient gradient propagation. The frozen layers highlighted with blue-colored boxes, indicating that these layers retain their pre-trained weights and are not updated during training. This allows the model to preserve generic, low-level features such as edges and textures, while the unfrozen layers at later stages of the architecture (represented by the non-colored blocks) are fine-tuned to learn domain-specific patterns relevant NHL subtype classification. The custom layers at the end of the network, which include batch normalization, ReLU activation, a dense layer, and a softmax layer, are used for final feature mapping and class probability output. By freezing early layers and adjusting deeper layers, the model balances feature generalization with specialization, enhancing classification performance while mitigating overfitting.

The value of layer freezing for the front and back layers was set to range from 10% to 100% sequentially. This strategy reduces the risk of overfitting and speeds up the training process. Let θ_f denote the parameters of the frozen layer and θ_t the parameters of the trainable layers. The model is fine-tuned by optimizing θ_t while keeping θ_f fixed. The final classification of image I is determined by a majority voting mechanism across its patches $\{P_1, P_2, \ldots, P_{16}\}$. Each patch P_i is classified independently, yielding predictions y_i. The final label Y is given by $Y = \arg max_{c\in\{CLL,FL,MCL\}} \sum_{i=1}^{16} \prod(y_i = c)$ where $\prod(y_i = c)$ is the indicator function that equals 1 if $y_i = c$ and 0 otherwise. This ensemble approach enhances the robustness and reliability of the classification outcomes.

IV. RESULT AND DISCUSSION

A. Performance of pretrained CNN models

A detailed comparison highlights the accuracy achieved by three pre-trained CNN models, fine-tuned with different optimizers, for classifying NHL in histopathological images, is summarized in Table II. The findings reveal distinct performance patterns across the models and optimizers, highlighting the impact of model architecture and optimization technique on classification accuracy.

DenseNet169 consistently achieves higher accuracy than MobileNetV2 and NASNetMobile across various optimizers, with its highest accuracy of 90.42% using Adagrad and 90.2% with SGD, suggesting that its densely connected layers promote feature reuse and efficient gradient flow, robust feature learning from histopathological images. Optimizer choice significantly impacts accuracy, with Adagrad and SGD yielding the best results for DenseNet169 due to Adagrad's adaptive learning rate and SGD's ability to avoid local minima through stochastic updates. In contrast, MobileNetV2 and NASNetMobile show varied performance across optimizers, with MobileNetV2 reaching 87.42% accuracy with Adagrad but dropping to 84.3% with Adadelta and Ftrl, while NASNetMobile peaks at 87.53% with SGD and drops to 85.75% with Adamax, indicating that the choice of optimizer affects their generalization capabilities, especially for these lighter architectures.

The superior performance of DenseNet169 can be attributed to its unique architecture, which includes dense connections that facilitate the efficient flow of information and gradients throughout the network. These connections allow the model to reuse features from earlier layers, making it particularly effective for complex classification tasks such as distinguishing NHL subtypes. DenseNet169's ability to achieve high accuracy across multiple optimizers demonstrates its versatility and robustness, making it more suitable for diverse patterns and high variability in histopathological images.

The patch-based approach used in this research also contributes to the models' performance by dividing large histopathological images into smaller, manageable patches. This method allows the models to focus on localized features that may indicate NHL, improving the detection of subtle morphological variations. By training the models on these patches, the network can learn to recognize critical features at different scales, thereby enhancing its overall accuracy. The efficacy of DenseNet169, particularly with Adagrad and SGD, suggests that combining its dense architecture with patch-based analysis enables the model to capture more detailed and localized information, leading to higher classification accuracy.

TABLE III
PERFORMANCE RESULT OF PRECISION, RECALL AND F1-SCORE

Optimizer	MobileNetV2			DenseNet169			NASNetMobile		
	P	R	F	P	R	F	P	R	F
Adam	0,86	0,86	0,86	0,86	0,86	0,86	0,86	0,86	0,86
SGD	0,86	0,85	0,85	0,90	0,90	0,90	0,87	0,87	0,87
RMSprop	0,85	0,85	0,85	0,89	0,89	0,89	0,81	0,87	0,87
AdamW	0,86	0,86	0,86	0,86	0,86	0,86	0,86	0,86	0,86
Adadelta	0,84	0,84	0,84	0,88	0,88	0,87	0,86	0,86	0,86
Adagrad	0,87	0,87	0,87	0,90	0,90	0,90	0,86	0,86	0,86
Adamax	0,84	0,84	0,84	0,89	0,88	0,88	0,85	0,85	0,85
Nadam	0,84	0,84	0,84	0,87	0,87	0,87	0,86	0,86	0,86
Ftrl	0,84	0,84	0,84	0,86	0,86	0,86	0,86	0,85	0,85

DenseNet169 consistently outperforms MobileNetV2 and NASNetMobile across various optimizers, achieving the highest precision, recall, and F1-scores, particularly with SGD and Adagrad, where all three metrics reach 0.90, as shown in Table III. This performance indicates that DenseNet169's architecture, with its dense connections facilitating feature reuse and efficient gradient flow, is well-suited for capturing complex patterns in histopathological images. The consistent performance across metrics suggests that DenseNet169 maintains a balanced ability to identify and retrieve relevant cases, demonstrating robustness in its classification capabilities. The choice of optimizer significantly impacts the models' performance, with SGD's stochastic updates and Adagrad's adaptive learning rate proving most effective for DenseNet169, likely due to their ability to enhance the model's generalization and minimize classification errors.

In contrast, MobileNetV2 and NASNetMobile show lower and more variable results, with their precision, recall, and F1-score generally lagging behind DenseNet169's. MobileNetV2 performs best with Adagrad (0.87 for all metrics). However, it drops to 0.84 with optimizers like Adadelta, Adamax, Nadam, and Ftrl, indicating that its simpler architecture may need help fully exploiting specific optimizers' benefits. NASNetMobile exhibits more variability in recall, reaching 0.87 with RMSprop and 0.85 with Adamax and Ftrl, suggesting that its ability to retrieve relevant instances is more sensitive to the optimization method. The differences across models and optimizers emphasize the importance of choosing the right combination, with DenseNet169 showing greater adaptability and resilience in handling the challenges of histopathological image classification.

The performance of the patch-based classification model for histopathological images is illustrated in the confusion matrix shown in Fig. 5. The model performs well, correctly classifying 259 out of 272 instances for CLL, 336 out of 336 instances for FL (with perfect accuracy), and 296 out of 304 instances for MCL. Misclassifications are minimal, with 13 CLL instances wrongly predicted as FL and only a few MCL cases misclassified as CLL or FL. The high accuracy, particularly for FL, highlights the robustness of the model, while the small number of errors demonstrates its effectiveness in distinguishing these cancer types.

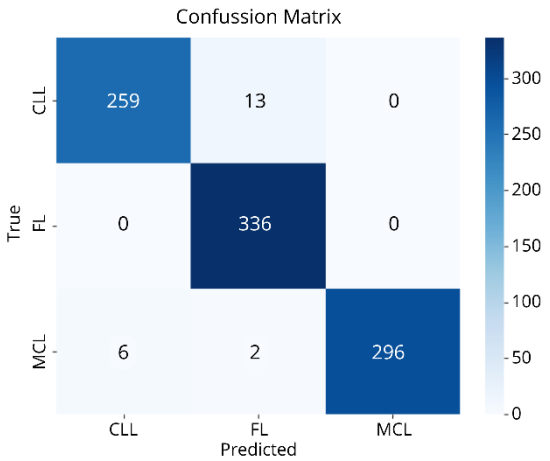

Fig. 5. Confusion matrix of image patching

The performance of a voting-based ensemble model for classifying histopathological images is depicted in the confusion matrix in Fig. 6. The model accurately classified 16 out of 17 CLL instances, with only one misclassified as MCL, while all 21 FL instances were correctly classified without error. For MCL, the model correctly identified 19 cases with no misclassifications. This performance demonstrates the effectiveness of the voting mechanism, which aggregates predictions from multiple classifiers, resulting in high accuracy and minimal errors across the categories.

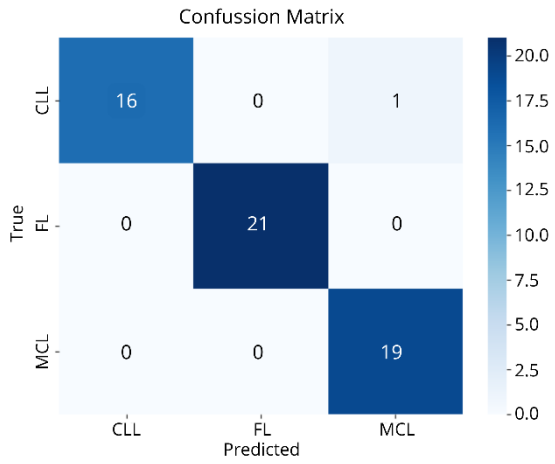

Fig. 6. Confusion matrix of image voting

Model performance is illustrated by the Receiver Operating Characteristic (ROC) curve in distinguishing CLL from other classes shown Fig. 7. The curve obtained a high Area Under the Curve (AUC) score of 0.99, indicating excellent discriminatory ability. The True Positive Rate (sensitivity) remains consistently high across varying False Positive Rates, demonstrating the model's robustness in correctly identifying CLL cases.

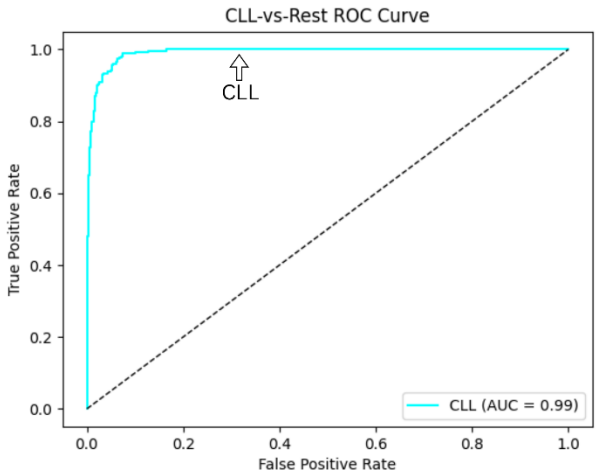

Fig. 7. ROC Curve for CLL Classification Against Other Subtypes

The model's performance in distinguishing FL from other subtypes is demonstrated in Fig. 8 through the ROC curve. Achieving an AUC score of 0.99, the model exhibits exceptional discriminatory capability, effectively classifying FL cases with high sensitivity across various false positive

rates. This result highlights the model's robustness and accuracy in handling challenging classification tasks.

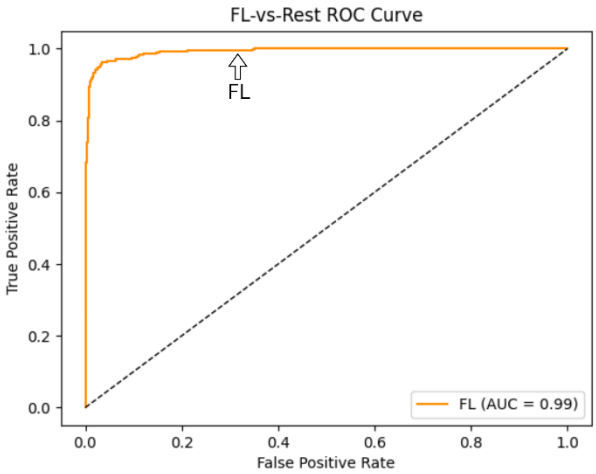

Fig. 8. ROC Curve for FL Classification Against Other Subtypes

The model's ability to distinguish MCL from other subtypes is represented in Fig. 9 through the ROC curve. With an AUC score of 0.99, the model demonstrates exceptional classification performance, maintaining high sensitivity across varying false positive rates. This result highlights the model's robustness and effectiveness in accurately identifying MCL cases despite the challenges associated with overlapping features among subtypes.

B. Impact of hyperparameter tuning

The choice of learning rate and batch size considerably affects the model's performance in classifying histopathological images for NHL, as highlighted in Table IV. A higher learning rate of 0.001 consistently yields better results across precision, recall, F1-score, and accuracy than a lower learning rate of 0.0001. Specifically, metrics remain above 0.90 with the higher learning rate, while they drop below 0.90 when the learning rate is reduced. This performance indicates that the higher learning rate enables more substantial weight updates, allowing the model to converge more effectively and capture essential patterns in the data. In contrast, the lower learning rate may cause slower convergence and inadequate parameter updates, leading to a suboptimal classification performance.

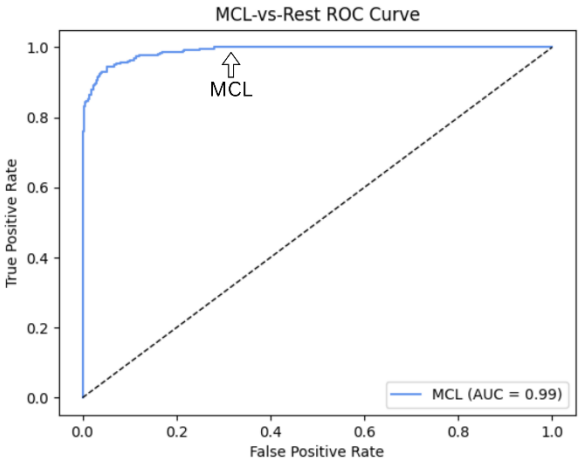

Fig. 9. ROC Curve for MCL Classification Against Other Subtypes

TABLE IV
RESULT OF HYPERPARAMETER TUNING

Learning rate	Batch size	Precision	Recall	F1-Score	Accuracy
0,001	8	0,9038	0,9036	0,9035	0,9053
0,001	16	0,9017	0,9023	0,9017	0,9031
0,001	32	0,9027	0,9025	0,9023	0,9042
0,0001	8	0,8985	0,8988	0,8983	0,8998
0,0001	16	0,8915	0,8917	0,8914	0,8931
0,0001	32	0,8748	0,8752	0,8738	0,8753

TABLE V
PERFORMANCE RESULT OF LAYER FREEZING ON THE BACK LAYERS

Value	Precision	Recall	F1-Score	Accuracy
10%	0,9387	0,9352	0,9366	0,9365
20%	0,9253	0,9226	0,9237	0,9243
30%	0,9247	0,9207	0,9223	0,922
40%	0,9408	0,9366	0,9377	0,9376
50%	0,9572	0,9541	0,9554	0,9555
60%	0,943	0,9416	0,9422	0,9421
70%	0,9408	0,9358	0,9377	0,9376
80%	0,9722	0,9711	0,9716	0,971
90%	0,9636	0,9618	0,9623	0,9621

TABLE VI
PERFORMANCE RESULT OF LAYER FREEZING ON THE FRONT LAYERS

Value	Precision	Recall	F1-Score	Accuracy
10%	0,9744	0,9727	0,9734	0,9733
20%	0,9442	0,9212	0,9268	0,9276
30%	0,9887	0,987	0,9878	0,9878
40%	0,9914	0,9909	0,9911	0,9911
50%	0,9819	0,9804	0,981	0,9811
60%	0,9853	0,984	0,9846	0,9844
70%	0,9782	0,9749	0,9762	0,9766
80%	0,9913	0,9905	0,9909	0,9911
90%	0,9884	0,9876	0,9879	0,9878

Regarding batch size, the results suggest that smaller batch sizes, especially 8 and 32, yield higher performance metrics compared to a batch size of 16. For instance, with a learning rate of 0.001, The best performance is observed with a batch size of 8, reaching an F1-score of 0.9035 and an accuracy of 0.9053. This performance indicates that smaller batches, which allow for more frequent updates to the model weights, can help the model generalize better. Although performance remains relatively stable across different batch sizes when using a learning rate of 0.001, the model is more responsive to changes in the learning rate than to batch size adjustments. Combining a learning rate of 0.001 and a batch size of 8 provides the optimal balance for achieving the highest classification performance.

The training and validation accuracy results are depicted in Fig. 10, offering a clear overview of the model's performance while training process. The graph shows how the model's training and validation accuracy changed over 100 epochs. The training accuracy (blue line) rapidly increases and reaches almost 100% by around 10 epochs, showing that the model effectively learns from the training data. The validation accuracy (red line) also increases quickly and stabilizes around 95%, slightly lower than the training accuracy, suggesting good but slightly overfitted performance. The small gap between the two accuracies indicates that the model generalizes well to unseen data, but the perfect training accuracy might hint at slight overfitting. Overall, the model shows strong performance with stable accuracy for both training and validation after the early epochs.

C. *Effectiveness of Layer Freezing and Majority Voting*

To determine the impact of layer freezing on the DenseNet169 model's performance, further experiments were conducted with two scenarios: layer freezing on the back layers and layer freezing on the front layers. The results are shown in Table V for layer freezing on the back layers and Table VI for layer freezing on the front layers. The best result was achieved by layer freezing 40% of the front layers with an accuracy of 99.11%.

The experiments showed distinct differences in performance based on which layers were frozen. Freezing the back layers preserved the specialized features learned during pre-training while allowing the model to adapt the initial layers to the new dataset. This scenario effectively maintained high performance across precision, recall, F1-score, and accuracy. Conversely, freezing the front layers allowed the deeper layers to specialize in identifying the specific characteristics of the lymphoma subtypes while leveraging the generalized features captured by the initial layers. Depending on the nature of the histopathological images and the specific requirements of the classification task, either approach could be advantageous. The choice between these two strategies should be informed by the dataset's characteristics and the specific features that need to be emphasized during training.

D. *Analysis of Misclassifications in NHL Subtypes*

This section identifies specific subtypes that are harder to classify due to overlapping histopathological features and morphological similarities. A successful prediction for a sample classified as Follicular Lymphoma (FL) shown in Fig. 11. The final classification aligns with the actual label (actual: FL, predicted: FL) based on the patch-based voting mechanism. The image is divided into 16 patches, each independently classified as FL, and the majority voting mechanism aggregates these patch-level predictions to determine the final label for the whole image. In this example, all patches were correctly predicted as FL, indicating the model's ability to consistently recognize the morphological features characteristic of FL. These features likely include uniform cellular structures, distinct nuclear patterns, and specific staining characteristics visible in the patches.

Fig. 10. Training and Validation Accuracy

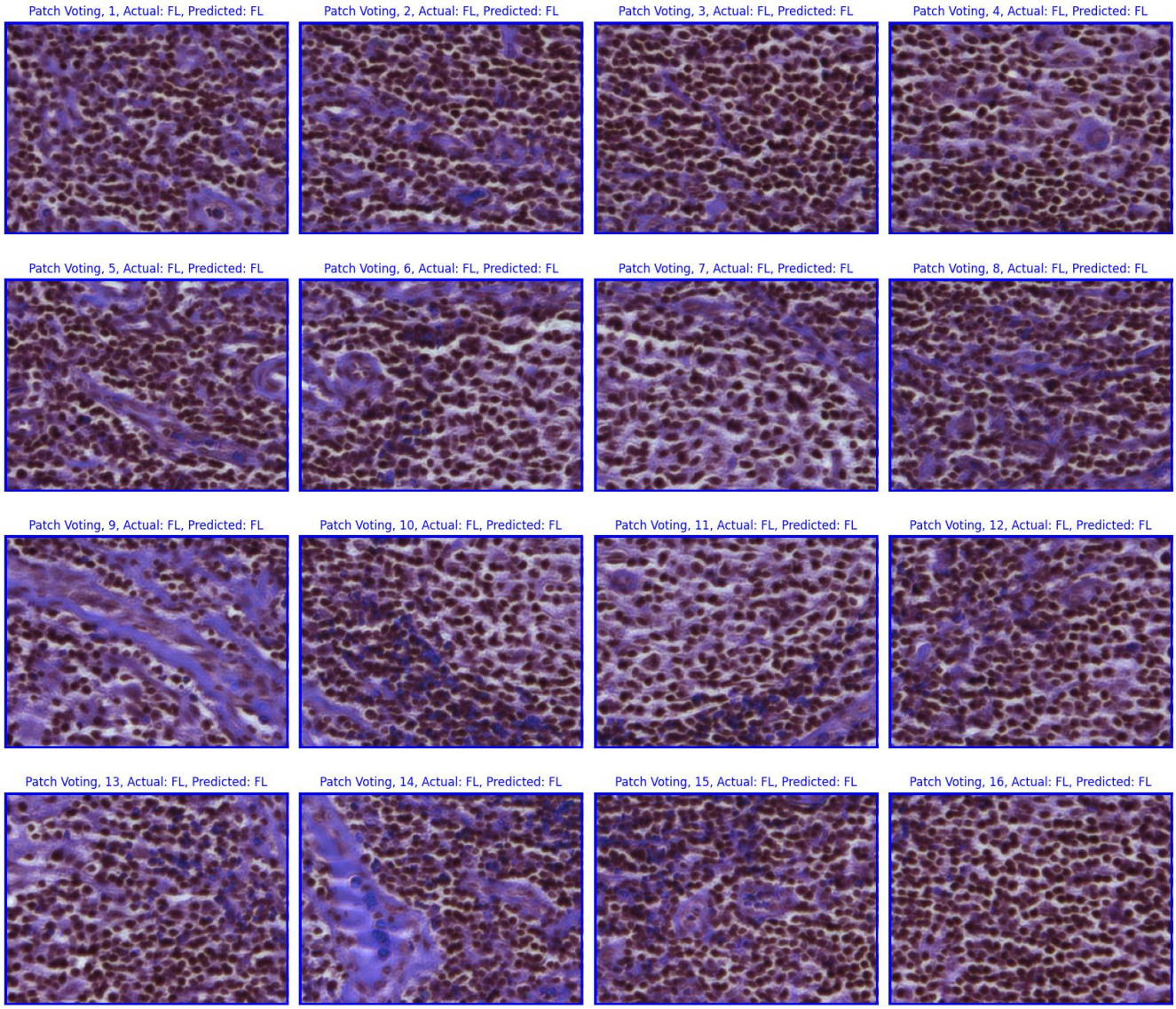

Fig. 11. Example of Successful Voting Prediction for FL

The misclassification case shown in Fig. 12, where the final prediction for the image, determined through the patch-based voting mechanism, is FL, while the actual label is MCL. The image is divided into 16 patches, with some patches correctly classified as MCL (blue boxes), but the majority are incorrectly classified as FL (red boxes) or CLL. This example highlights the model's difficulty in distinguishing between subtypes with overlapping histopathological features, demonstrating the need for improved feature extraction or preprocessing to address such challenges.

The patches classified as FL or CLL suggest that the model may not have fully learned the distinguishing features of MCL, likely due to a lack of sufficient representation or variability of MCL samples during training. Noise and artifacts in the patches may also obscure critical features, further contributing to misclassification.

E. Comparison with previous method

A comparison of NHL classification performance between our method and existing studies is presented in Table VII. It indicates that our method, using patch-based DenseNet169 with layer freezing and majority voting, achieves an accuracy of 99.1%, which is on par with the performance of the patch-based GoogLeNet. This high level of accuracy demonstrates the efficacy of layer freezing in the CNN architecture, allowing the model to retain low-level features while focusing on learning high-level, domain-specific features.

Our proposed method, the patch-based DenseNet169 with layer freezing and majority voting, stands out as the best compared to other approaches despite having the same accuracy as Patch-based GoogLeNet (99.1%). First, the integration of layer freezing allows us to leverage the strengths of pre-trained models by retaining the low-level features learned from large datasets while fine-tuning only the higher layers to adapt to the specific characteristics of NHL images. This technique significantly reduces the risk of overfitting, especially when dealing with smaller medical datasets, improving the model's robustness. Additionally, the majority voting mechanism enhances the classification by aggregating predictions from individual image patches, making the model more resilient to noise or misclassified patches and ensuring more reliable final predictions.

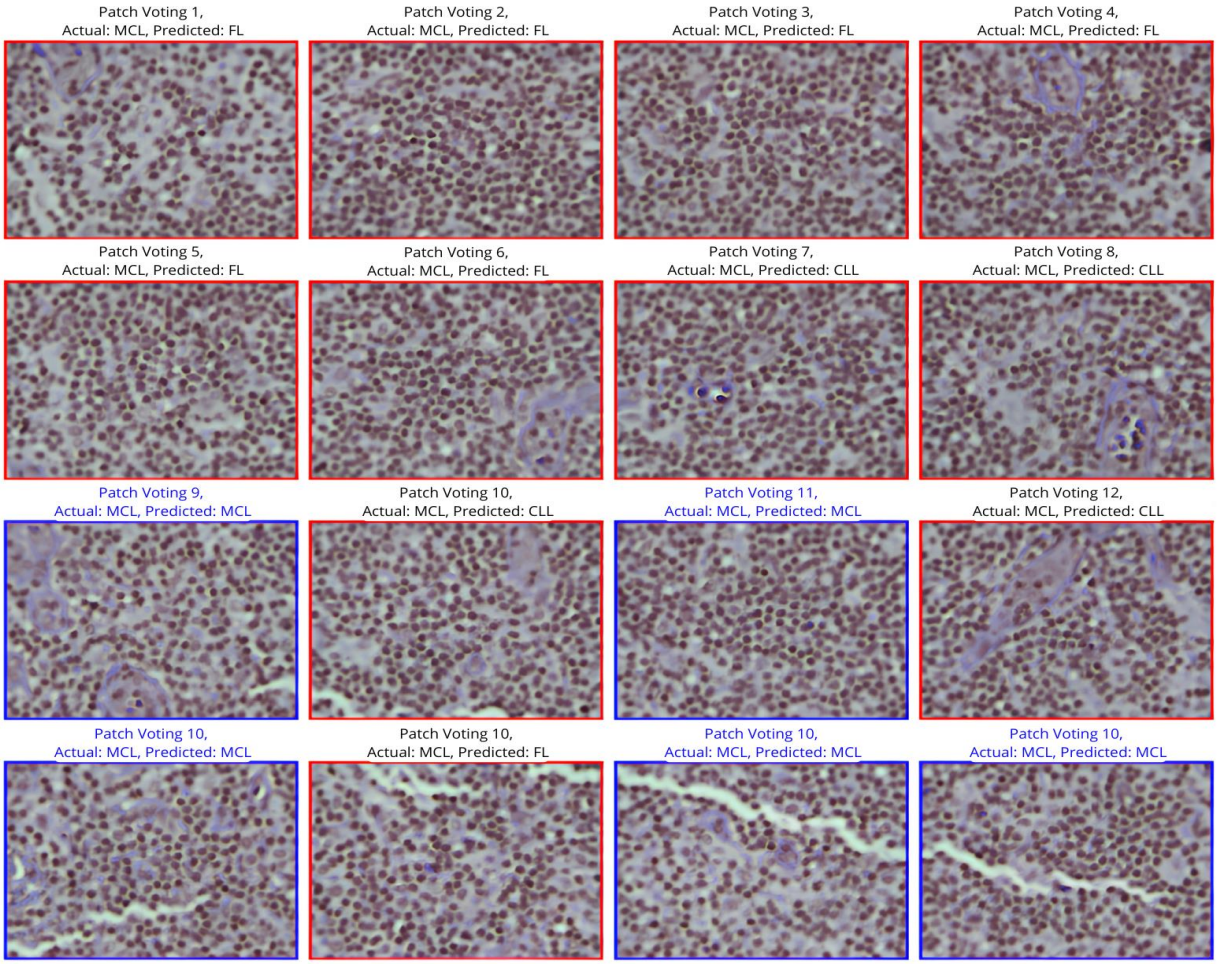

Fig. 12. Example of NHL Misclassification

TABLE VII
RESULT OF OUR METHOD AND EXISTING STUDIES

Method	Accuracy (%)
Patch-based GoogLeNet [27]	99.1
ResNet50 [36]	96.6
Gradient Boosting Decision Tree [40]	93.2
Fractal features and Hermite polynomial [29]	97.6
Patch-based DenseNet169 with layer freezing and majority voting [Ours]	99.1

Compared to ResNet50 and the Gradient Boosting Decision Tree, which achieved lower accuracy (96.6% and 93.2%, respectively), our method balances classification accuracy with computational efficiency, mainly when dealing with high-dimensional medical images. Furthermore, while the fractal features and Hermite polynomial method also show strong performance (97.6%), it relies heavily on handcrafted features, making it less flexible and adaptable than our deep learning-based approach, which automatically extracts and refines relevant features without the need for manual intervention. Overall, our method's combination of cutting-edge deep learning techniques, transfer learning, and ensemble strategies makes it highly effective for precise and efficient NHL detection.

F. Limitation of the study

The primary limitation of this research is the relatively small size of the IICBU 2008 dataset, which includes only 374 images and three NHL subtypes, potentially limiting the generalizability of the results to broader and more diverse clinical datasets. Additionally, while the layer freezing and majority voting mechanisms improve classification performance, they may introduce computational overhead, making real-time clinical applications more challenging. The lack of validation on external datasets further restricts the assessment of the model's robustness across varying data sources, and there is a potential risk of overfitting due to the model's near-perfect training accuracy, which may not fully reflect real-world conditions.

V. CONCLUSION

This research successfully applies a patch-based histopathological image classification method using a pre-trained DenseNet169 model with a layer-freezing strategy and majority voting for NHL subtype detection. Through meticulous preprocessing, including the division of images into 4 × 4 patches and the use of Adagrad optimizer alongside a majority voting algorithm, the model achieved exceptional performance metrics, with an accuracy of 99.11% and precision, recall and F1-score of 99.14%, 99.09%, and 99.11%, respectively. The hyperparameter tuning results further validated the efficacy of the chosen model and configurations, with the optimal performance observed at a

learning rate of 0.001 and a batch size of 8. These findings underscore the potential of integrating advanced CNN architectures and innovative strategies to enhance the accuracy and efficiency of histopathological image analysis, thereby improving diagnostic workflows and clinical outcomes for NHL.

Further validation of our model on more extensive and diverse datasets and integration into clinical practice will be essential to fully realizing its potential impact. Additionally, ongoing refinement and optimization of the model architecture and training processes will continue to enhance its performance and generalizability across different medical imaging tasks.

REFERENCES

[1] F. Holdsworth, D. Worku, A. le Bretton, C. Vella, and E. Walker, "A guide to Hodgkin and non-Hodgkin lymphomas: similarities and differences," *Br. J. Nurs.*, vol. 30, no. 17, 2021.

[2] E. Sedeta *et al.*, "Epidemiology of Non-Hodgkin Lymphoma: Global Patterns of Incidence, Mortality, and Trend," *Blood*, vol. 140, pp. 5234–5235, 2022, doi: https://doi.org/10.1182/blood-2022-158830.

[3] M. G. Hanna *et al.*, "Whole slide imaging equivalency and efficiency study: experience at a large academic center," *Mod. Pathol.*, vol. 32, no. 7, pp. 916–928, 2019, doi: 10.1038/s41379-019-0205-0.

[4] L. Hou, D. Samaras, T. M. Kurc, Y. Gao, J. E. Davis, and J. H. Saltz, "Patch-Based Convolutional Neural Network for Whole Slide Tissue Image Classification," in *Proceedings of the IEEE Computer Society Conference on Computer Vision and Pattern Recognition*, 2016, vol. 2016-Decem, pp. 2424–2433, doi: 10.1109/CVPR.2016.266.

[5] F. Ullah, A. Salam, M. Abrar, and F. Amin, "Brain Tumor Segmentation Using a Patch-Based Convolutional Neural Network: A Big Data Analysis Approach," *Mathematics*, vol. 11, no. 7, pp. 1–18, 2023, doi: 10.3390/math11071635.

[6] M. Mabuchi and T. Ishikawa, "Patch-based Privacy Preserving Neural Network for Vision Tasks," in *Proceedings - 2023 IEEE Winter Conference on Applications of Computer Vision, WACV 2023*, 2023, pp. 1550–1559, doi: 10.1109/WACV56688.2023.00160.

[7] I. Hirra *et al.*, "Breast Cancer Classification from Histopathological Images Using Patch-Based Deep Learning Modeling," *IEEE Access*, vol. 9, pp. 24273–24287, 2021, doi: 10.1109/ACCESS.2021.3056516.

[8] I. Hirra *et al.*, "Breast Cancer Classification from Histopathological Images Using Patch-Based Deep Learning Modeling," *IEEE Access*, vol. 9, no. 11, pp. 24273–24287, 2021, doi: 10.1109/ACCESS.2021.3056516.

[9] A. Zawisza, M. Tabakov, K. Karanowski, and K. Galus, "Morphological Analysis of Histopathological Images Using Deep Learning," in *Communications in Computer and Information Science*, 2021, vol. 1463, no. September, pp. 134–145, doi: 10.1007/978-3-030-88113-9_11.

[10] K. Kawattikul, K. Sermsai, and P. Chomphuwiset, "Improving the sub-image classification of invasive ductal carcinoma in histology images," *Indones. J. Electr. Eng. Comput. Sci.*, vol. 26, no. 1, pp. 326–333, 2022, doi: 10.11591/ijeecs.v26.i1.pp326-333.

[11] H. Chen, X. Zhang, and T. Zhou, "Multiple Instance Learning Research for the Classification of Lung Cancer in CT Diagnosis," *Eng. Lett.*, vol. 32, no. 7, pp. 1313–1324, 2024.

[12] R. K. Paul, A. Vishwakarmaw, and S. Chandran, "An Aquatic Image Compression Scheme based on Optimized Deep Convolutional Autoencoder," *IAENG Int. J. Comput. Sci.*, vol. 51, no. 2, pp. 83–90, 2024.

[13] M. Dörrich *et al.*, "Explainable convolutional neural networks for assessing head and neck cancer histopathology," *Diagn. Pathol.*, vol. 18, no. 1, pp. 1–11, 2023, doi: 10.1186/s13000-023-01407-8.

[14] A. K. Pandey, D. Jain, T. K. Gautam, and J. S. Kushwah, "Tomato Leaf Disease Detection using Generative Adversarial Network-based," *Eng. Lett.*, vol. 32, no. 5, pp. 965–973, 2024.

[15] R. Schmitz *et al.*, "Multi-scale fully convolutional neural networks for histopathology image segmentation: From nuclear aberrations to the global tissue architecture," *Med. Image Anal.*, vol. 70, 2021, doi: 10.1016/j.media.2021.101996.

[16] A. Saber, A. G. Hussien, W. A. Awad, A. Mahmoud, and A. Allakany, "Adapting the pre-trained convolutional neural networks to improve the anomaly detection and classification in mammographic images," *Sci. Rep.*, vol. 13, no. 1, pp. 1–18, 2023, doi: 10.1038/s41598-023-41633-0.

[17] M. Krichen, "Convolutional Neural Networks: A Survey," *Computers*, vol. 12, no. 8, pp. 1–41, 2023, doi: 10.3390/computers12080151.

[18] L. Lu and B. J. Daigle, "Prognostic analysis of histopathological images using pre-trained convolutional neural networks: application to hepatocellular carcinoma," *PeerJ*, vol. 12, 2020.

[19] T. L. Huang *et al.*, "Transfer learning with CNNs for efficient prostate cancer and BPH detection in transrectal ultrasound images," *Sci. Rep.*, vol. 13, no. 1, pp. 1–9, 2023, doi: 10.1038/s41598-023-49159-1.

[20] M. Tan and Q. V. Le, "EfficientNet: Rethinking model scaling for convolutional neural networks," in *36th International Conference on Machine Learning, ICML 2019*, 2019, vol. 2019-June, pp. 10691–10700.

[21] C. Gu and M. Lee, "Deep Transfer Learning Using Real-World Image Features for Medical Image Classification, with a Case Study on Pneumonia X-ray Images," *Bioengineering*, vol. 11, no. 4, 2024, doi: 10.3390/bioengineering11040406.

[22] C. L. Srinidhi, O. Ciga, and A. L. Martel, "Deep neural network models for computational histopathology: A survey," *Med. Image Anal.*, vol. 67, 2021, doi: 10.1016/j.media.2020.101813.

[23] H. Mewada, "Extended Deep-Learning Network for Histopathological Image-Based Multiclass Breast Cancer Classification Using Residual Features," *Symmetry (Basel).*, vol. 16, no. 5, p. 507, 2024, doi: 10.3390/sym16050507.

[24] S. Kosaraju, J. Park, H. Lee, J. W. Yang, and M. Kang, "Deep learning-based framework for slide-based histopathological image analysis," *Sci. Rep.*, vol. 12, no. 1, pp. 1–15, 2022, doi: 10.1038/s41598-022-23166-0.

[25] K. Roy, D. Banik, D. Bhattacharjee, and M. Nasipuri, "Patch-based system for Classification of Breast Histology images using deep learning," *Comput. Med. Imaging Graph.*, vol. 71, pp. 90–103, 2019.

[26] L. Shamir, N. Orlov, D. M. Eckley, T. J. Macura, and I. G. Goldberg, "IICBU 2008 - A Proposed Benchmark Suite for Biological Image Analysis," *Med Biol Eng Comput.*, vol. 46, no. 9, pp. 943–947, 2008, doi: 10.1007/s11517-008-0380-5.IICBU.

[27] J. Bai, H. Jiang, S. Li, and X. Ma, "NHL Pathological Image Classification Based on Hierarchical Local Information and GoogLeNet-Based Representations," *Biomed Res. Int.*, vol. 2019, pp. 1–13, 2019, doi: 10.1155/2019/1065652.

[28] M. Z. do Nascimento, A. S. Martins, T. A. A. Tosta, and L. A. Neves, "Lymphoma images analysis using morphological and non-morphological descriptors for classification," *Comput. Methods Programs Biomed.*, vol. 163, pp. 65–77, 2018.

[29] A. S. Martins *et al.*, "Colour Feature Extraction and Polynomial Algorithm for Classification of Lymphoma Images," in *Progress in Pattern Recognition, Image Analysis, Computer Vision, and Applications*, 2019, pp. 262–271, doi: 10.1007/978-3-030-33904-3.

[30] H. E. Kim, A. Cosa-Linan, N. Santhanam, M. Jannesari, M. E. Maros, and T. Ganslandt, "Transfer learning for medical

image classification: a literature review," *BMC Med. Imaging*, vol. 22, no. 1, pp. 1–13, 2022, doi: 10.1186/s12880-022-00793-7.

[31] Y. Wang, B. Wu, and Z. Duan, "Insulator Self-Explosion Detection Based on Mixed Samples and Transfer Learning," *IAENG Int. J. Comput. Sci.*, vol. 51, no. 10, pp. 1579–1586, 2024.

[32] A. W. Salehi *et al.*, "A Study of CNN and Transfer Learning in Medical Imaging: Advantages, Challenges, Future Scope," *Sustainability*, vol. 15, pp. 1–28, 2023.

[33] W. Teng, H. Zhang, and Y. Zhang, "X-ray Security Inspection Prohibited Items Detection Model based on Improved YOLOv7-tiny," *IAENG Int. J. Appl. Math.*, vol. 54, no. 7, pp. 1279–1287, 2024.

[34] O. Ciga, T. Xu, S. Nofech-Mozes, S. Noy, F. I. Lu, and A. L. Martel, "Overcoming the limitations of patch-based learning to detect cancer in whole slide images," *Sci. Rep.*, vol. 11, no. 1, p. 8894, 2021, doi: 10.1038/s41598-021-88494-z.

[35] M. Moscalu *et al.*, "Histopathological Images Analysis and Predictive Modeling Implemented in Digital Pathology—Current Affairs and Perspectives," *Diagnostics*, vol. 13, no. 14, pp. 1–21, 2023, doi: 10.3390/diagnostics13142379.

[36] S. Panigrahi, B. S. Nanda, R. Bhuyan, K. Kumar, S. Ghosh, and T. Swarnkar, "Classifying histopathological images of oral squamous cell carcinoma using deep transfer learning," *Heliyon*, vol. 9, no. 3, p. e13444, 2023, doi: 10.1016/j.heliyon.2023.e13444.

[37] Z. Wang *et al.*, "ResNet for Histopathologic Cancer Detection, the Deeper, the Better?," *J. Data Sci. Intell. Syst.*, vol. 00, no. January, pp. 1–8, 2023, doi: 10.47852/bonviewjdsis3202744.

[38] S. Saha, T. Chakraborty, R. Bin Sulaiman, and T. Paul, "A Comparative Analysis of CNN-Based Pretrained Models for the Detection and Prediction of Monkeypox," *arXiv:2302.10277*, pp. 1–10, 2023.

[39] A. Pal, J. K. Seth, A. Tyagi, A. Haider, and A. Mishra, "An Efficient Brain Tumor Detection Using Ensemble Learning," *Educ. Adm. Theory Pract.*, vol. 30, no. 5, pp. 9954–9968, 2024, doi: 10.53555/kuey.v30i5.4686.

[40] T. P. de Faria, M. Z. do Nascimento, and L. G. A. Martins, "A Method For Multiclass Lymphoma Classification Based on Morphological and Non-Morphological Descriptors," in *Workshop de Visão Computacional*, 2021, no. November, pp. 184–189, doi: 10.5753/wvc.2021.18911.